Available online at www.sciencedirect.com

ScienceDirect

journal homepage: www.elsevier.com/locate/he

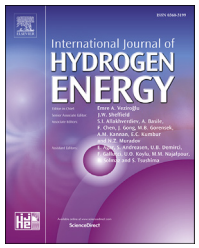

Hydrogen from glycerol steam reforming with a platinum catalyst supported on a SiO_2-C composite

Ivana N. Buffoni [a,b], *Martín N. Gatti* [a,b], *Gerardo F. Santori* [a,b], *Francisco Pompeo* [a,b], *Nora N. Nichio* [a,b,*]

[a] *Facultad de Ingeniería, Universidad Nacional de La Plata, 1 esq 47, 1900, La Plata, Argentina*
[b] *CINDECA, Facultad de Ciencias Exactas, Universidad Nacional de La Plata-CONICET, 47 no 257, 1900, La Plata, Argentina*

ARTICLE INFO

Article history:
Received 6 November 2016
Received in revised form
30 March 2017
Accepted 9 April 2017
Available online 28 April 2017

Keywords:
Hydrogen
Glycerol
Steam reforming
Platinum

ABSTRACT

This work studies 2 wt% Pt catalysts. The support is a SiO_2-C composite whose main features are a high specific surface due to its mesoporosity, a higher thermal stability than the C support, and the absence of surface acid sites which could promote the dehydration reactions that produce coke precursors. The Pt/SiO_2-C catalyst has very small metallic particles (d_{va} = 1.37 nm) that favor the C–C bond cleavage reactions which allow obtaining total gas conversion at 450 °C. With this catalyst, it is possible to obtain high yields to H_2, between 4 and 5, which indicates that the active sites promote the WGS reaction, even with glycerol concentrations of 30 and 50%. Pt/SiO_2-C is a very stable catalyst since it loses only 10% of its initial activity after 66 h on stream and is resistant to sintering and coke deposition.

Introduction

The growing demand for fuels and the global concerns for environmental issues have motivated the development of new technologies to employ renewable raw materials. In Argentina, the existing legal framework has given a very strong impulse to biodiesel production; in 2016, the internal biodiesel market was of around 4.5×10^6 tons, being one of the world's main producers [1,2]. This has generated an excess of glycerol in the market which has spurred the study of new applications to allow its transformation into products with higher added value [3]. Glycerol steam reforming (GSR) could be a promising alternative since the process would not represent major changes with respect to the current industrial process to obtain hydrogen [4]. The feasibility of producing hydrogen by GSR has been studied by different authors and several recent reviews report the state of the art on this topic [5–7]. GSR requires large amounts of energy to vaporize reactants. For this reason, it is significantly important to decrease the reforming temperature in order to achieve a sustainable technological application.

The reactions present in glycerol GSR are the combination of glycerol decomposition (Eq. (1)) with the water–gas shift reaction (WGS, Eq. (2))

$$\text{Glycerol decomposition}: \quad C_3H_8O_3 \xrightarrow{H_2O} 3CO + 4H_2 \qquad (1)$$

$$\text{Water} - \text{Gas Shift(WGS)reaction}: \quad CO + H_2O \leftrightarrow CO_2 + H_2 \qquad (2)$$

* *Corresponding author*. CINDECA, Facultad de Ciencias Exactas, Universidad Nacional de La Plata-CONICET, 47 no 257, 1900, La Plata, Argentina. Fax: +54 221 4254277.
E-mail address: nnichio@quimica.unlp.edu.ar (N.N. Nichio).
http://dx.doi.org/10.1016/j.ijhydene.2017.04.047

Therefore, the overall reaction of glycerol reforming can be described as follows (eq. (3))

$$C_3H_8O_3 + x\,H_2O \leftrightarrow (3-x)CO + xCO_2 + (4+x)H_2 \quad (3)$$

where x varies in the ranges from 0 to 3, 0 indicates glycerol decomposition and 3 glycerol reforming. Other secondary reactions can also take place, like methanation and carbon formation [8,9].

Following the pioneering work of J.A. Dumesic and his research group in 2006, several authors have studied a great variety of catalyst formulations applied to an ample temperature range from 300 to 800° C [10–16]. Catalysts based on noble metals including Pt [17–19], Pd [20], Ir [21], Rh [22,23] and Ru [24,25] and on non-noble metals (Ni and Co) [26,27] have been studied.

Of the metals studied, those that stand out are noble metals such as Pt. They are preferred because of their greater selectivity to the cleavage of C–C bonds. Soares et al. analyzed the effect of the support on Pt-based catalysts [10]. In the catalysts supported on γ-Al_2O_3, ZrO_2, CeO_2/ZrO_2 and MgO/ZrO_2, the WGS reaction is favored. However, these catalysts present strong deactivation after 20 h on stream at atmospheric pressure and 350 °C. Soares et al. demonstrated that the main cause of deactivation of the Pt catalyst supported on oxides is the dehydration on the support sites which leads to the formation of unsaturated hydrocarbons that afterwards form carbonaceous species on the Pt surface. The only catalyst that did not deactivate under such conditions was the Pt catalyst supported on C [10].

In this regard, we studied the effect of the support (SiO_2, α-Al_2O_3, Ce-Zr-αAl_2O_3 and ZrO_2) on Pt catalysts [28]. The Pt/SiO_2 catalyst showed the best activity and selectivity to H_2 at 450 °C with a reaction mixture to 10 wt% of glycerol. Besides, we determined that the materials with surface acidity properties promote lateral reactions and the presence of intermediaries such as acetol (coming from the cleavage of the C–O bond on the metallic site or through dehydration on the support) leads to the formation of coke and later, to the deactivation of the catalyst.

Simonetti et al. [11] studied the GSR at 280 °C using carbon-supported platinum (PtC) and platinum–rhenium (Pt-Re/C) catalysts with different Re content. They demonstrated that the bimetallic Pt-Re/C catalysts with atomic Pt:Re $\leq$ 1 are 5 times more active. Afterwards, Wei et al. [18] reported the fundamental surface properties of Pt/C and Pt-Re/C catalysts and their correlation with catalytic performance in GSR. They determined that the addition of Re increases the catalytic activity, H_2/CO_x ratio, and CO_2 selectivity. This was attributed to Re oxidation by the presence of water vapor, supplying a redox site for the CO spillover, on which CO can easily desorb or react to form CO_2.

Clearly, the main challenge for GSR is to reduce the carbon deposition. Cheng et al. reported that the formation of coke on Co-Ni-Al_2O_3 catalysts is strongly dependent on glycerol concentration but weakly dependent on the amount of water vapor [16].

Working with Ni catalysts, Gong et al. established that the smaller Ni particle size and stronger MSI could suppress carbon deposition, and thus improve the catalyst stability [29,30]. Considering the severe deactivation due to coke formation, these authors proposed three strategies to improve stability: i-the preparation of highly dispersed nickel catalysts with strong metal–support interaction, ii-the promotion in the mobility of the surface oxygen in order to allow the removal of the coke deposits, and iii-further research work on CO_2 sorption enhanced reforming (CO_2-SER) [31].

Chiodo et al. [32] revealed that coke deposits of different morphology are formed upon a Rh/Al_2O_3 catalyst, depending on the reaction temperature. High reaction temperature (>650 °C) promotes the formation of encapsulating carbon which negatively reflects on catalyst stability. For this reason, a catalyst presents a lower yield at high temperatures even though reforming is thermodynamically more favorable.

Montini et al. [12] doped a Pt/Al_2O_3 catalyst with basic additives and achieved good stability for Pt/La_2O_3/Al_2O_3, whereas Pt/CeO_2/Al_2O_3 deactivated abruptly after 20 h under similar conditions. These authors argued that the deactivation observed can be attributed to the coke deposition upon the active sites and indicated that an appropriate composition is necessary for the preparation of high-yield Pt catalysts.

Araque et al. [33] studied catalysts of Co and CoRh supported on CeZr. All the catalysts showed a sharp drop in the yield to H_2 with the reaction time. The most stable catalyst was CoRh; however, the conversion to gas products dropped after 16 h on stream. The greatest cause of deactivation was attributed to the formation of C_2H_4 as a consequence of the loss of catalyst capacity to enhance the cleavage of C–C bonds.

Pastor-Pérez et al. [4] have recently reported the effect of Sn addition to Pt/C catalysts with different Pt:Sn ratio on the production of hydrogen from GSR at 350 °C. It was found that Sn addition promotes the CO oxidation reaction producing H_2-rich gas streams and inhibits reactions that form coke precursors; however, the presence of Sn becomes detrimental if a too high amount of this promoter is present.

Through the analysis of the literature, the importance of the support's role in the GSR becomes clear. The activated carbon supports present several advantages such as a high surface area, the presence of different functional surface groups and an easy recovery of the metals by burning off the support. However, they also present certain disadvantages such as a lower metal-support interaction compared with classical oxides like SiO_2 and Al_2O_3. Even though they present high surface area, a great part of this area could be given by micropores that cause diffusion problems limiting both the deposition of the active phases in these pores and the reactants access. Besides, even though carbon presents a variety of oxygenated surface groups, the nature of the activated carbon is amorphous and this could affect the metallic dispersion.

The aim of the present work is to explore the behavior of the SiO_2-C composite synthesized by the sol–gel method as support, studying its structural properties and surface acidity. Pt catalysts supported on C, SiO_2 and SiO_2-C were prepared in order to evaluate the effect of the support and the metallic dispersion on the catalytic activity and stability in the GSR at 450 °C.

Experimental

Catalyst preparation

A SiO_2-C composite, a carbonaceous support obtained from the composite, and a commercial silica were used as catalytic supports. The SiO_2-C support was prepared by co-gellification of TEOS (TEOS, SILBOND 40 –AKZO Chemicals) and a phenolic resin (RL 43003, ATANOR S.A.). This material was calcined at 1500 °C (at 5 °C°min^{-1}) for 3 h in a reducing atmosphere [34].

The carbonaceous support denoted as C was obtained from SiO_2-C. The composite was submerged into 20 wt% HF, and removed from the solution after 30 min. Then, it was washed with distilled water, eliminating the residual H_2F_6Si by heating at 400 °C [34].

Besides, a commercial SiO_2, Degussa (Aerosil 200), was used as support.

The Pt/SiO_2-C and Pt/C catalysts were prepared by impregnation with H_2PtCl_6 (Aldrich) in ethanol solution at 60 °C during 12 h. The solids were dried at 120 °C for 12 h. Li et al. have reported that the decomposition of H_2PtCl_6 in $PtCl_2$ occurs at temperatures below 250 °C and then, the decomposition of $PtCl_2$ occurs at 300 °C [35]. Thus, calcination was carried out at 300 °C in air flow for 2 h.

In order to obtain a Pt/SiO_2 catalyst with high metallic dispersion, the preparation method by ionic exchange was employed. Since the isoelectric point of SiO_2 is between 1 and 2, $Pt(NH_3)_4Cl_2$ in aqueous solution had to be used as precursor. For the preparation by cationic exchange, the silica was suspended in NH_4OH under stirring prior to the addition of the $[Pt(NH_3)_4]Cl_2$ solution, having a concentration so as to obtain 2 wt% Pt exchanged on the silica. The solid was kept under stirring for 24 h at 25 °C, in order to be able to obtain a uniform distribution of platinum over the silica surface, as indicated by Goguet et al. [36]. Subsequently, the suspension was separated by filtration under vacuum. The solid was repeatedly washed and dried at 105 °C for 12 h. According to a report by Richard et al., the $Pt(NH_3)_4Cl_2$ precursor salt first decomposed into $Pt(NH_3)_2Cl_2$ and NH_3 at 300–350 °C, and then a second decomposition occurred in the 350–450 °C region where NH_3 and HCl were eliminated [37]. In this way, calcination was carried out in air flow (50 mL min^{-1}) at 500 °C for 2 h.

Catalyst characterization

The platinum content was 2 wt% nominal. The Pt content of samples was determined by atomic absorption spectrometry (AAS). The calibration curve method was used, with standards prepared in the laboratory. The equipment utilized was an IL Model 457 spectrophotometer, with a single channel and double beam. The light sources were hollow monocathode lamps.

Adsorption–desorption measurements were performed for a textural characterization. Surface area measurements, the Brunauer–Emmett–Teller (BET) multipoint method and textural analysis, were obtained using a Micromeritics ASAP 2020 equipment. The samples were pretreated under vacuum in two 1 h stages at 100 and 300 °C. The textural characterization involved specific surface measurements, pore size distribution determination, total pore volume, and micro and mesopore volume values. Pore size distribution was calculated from the adsorption branch of each isotherm using the model proposed by Barret, Joyner and Halenda (BJH), assuming a pore model of "slit" type. Micropore surface (S_{micro}) and micropore volume (V_{micro}) were estimated using the t-plot method, while the mesopore surface (S_{meso}) was calculated by subtracting S_{micro} from S_{BET}.

The point of zero charge (ZPC) was determined by the titration method using a Model Keithley 616 with Metrohom calomel electrodes. KCl solutions were used as supporting electrolytes.

Temperature-programmed reduction tests (TPR) were performed using a conventional dynamic equipment and the response was measured using a thermal conductivity detector. The feed flow was H_2/N_2 ratio of 1/9 and the heating rate was 10 °C min^{-1} from room temperature up to 1000 °C.

The temperature-programmed desorption (TPD) and temperature-programmed oxidation (TPO) were performed in a Micromeritics (Autochem II 2920) equipment. The TPD was performed from 50 °C to 800 °C at a heating rate of 10 °C°min^{-1} in Ar flow and the desorbed amount of CO and CO_2 was followed by a quadrupole mass spectrometer.

TPO/TGA (temperature-programmed oxidation by thermogravimetry) was performed in a Shimadzu TGA 50 instrument. The samples of 0.01 g were used with an air flow of 40 cm^3 min^{-1} and heating of 10 °C°min^{-1} from room temperature to 850 °C.

XRD patterns were recorded on a Philips 3020 powder diffractometer, using Cu Kα radiation (λ = 1.5418 Å, intensity = 40 mA, and voltage = 35 kV). The patterns were recorded in the range of 2θ = 20°–70°.

The XPS analysis was carried out in a multitechnique system (Specs), equipped with a dual Mg/Al X-ray source and a hemispherical PHOIBOS 150 analyzer operating in the fixed analyzer transmission (FAT) mode. The spectra were obtained with a pass energy of 30 eV and an Al Kα anode operating at 200 W. The samples were subjected to a reduction treatment for 10 min at 400 °C in a H_2-5%/Ar stream. The Pt/SiO_2 sample was reduced in situ for the XPS measurements, while the Pt/SiO_2-C and Pt/C samples (fresh and used ones) could not be pills and so they had to be reduced ex-situ.

Transmission electron microscopy (TEM) images were taken by means of a TEM JEOL 100 C instrument, operating at 200 KV. A graphite pattern was used for calibration. To estimate the average particle size (d_{va}), the particles were considered spherical and the diameter volume-area was calculated. Histograms of particle size distribution arose from microphotographs using the technique of clear field image.

Acid–base properties of supports were determined by an indirect method consisting of the test of isopropanol (IPA) decomposition [38]. This reaction was tested in a continuous-flow fixed-bed reactor between 150 and 400 °C, atmospheric pressure, feed 4.5% IPA in Helium, with a flow 40 cm^3 min^{-1}.

The carbon deposits were studied using Laser Raman Spectroscopy (LRS) in a LabRAM HR UV 800 (Horiba/JobinYvon) instrument, laser HeeNe (λ = 632 nm), CCD detector and an OLYMPUS microscope, model BX41. The measurements of the samples, diluted in KBr, were taken with a 100× magnification

and the scattered light was collected through a confocal hole of 100 mm.

Catalytic tests

The experimental equipment used for the reaction test of glycerol steam reforming is a fixed-bed quartz reactor (i.d. = 8 mm) operated isothermally at atmospheric pressure. Prior to the reaction, the catalysts were reduced in situ at 500 °C (heating rate of 10 °C°min^{-1}) for 1 h in pure H_2 flow of 30 mL min^{-1}. The aqueous solution of glycerol (from 10 to 50 wt %) was injected to the reactor by a HPLC pump (Waters 590). Nitrogen was used as carrier gas (50–100 mL min^{-1}).

The analysis of gaseous reaction products was performed with a Shimadzu GC-8A (TCD detector) gas chromatograph equipped with a HayeSep DB 110-120 column.

The glycerol conversion to gaseous products (CO, H_2, CO_2 and CH_4) was denoted as X_G % and it was calculated based on the following equation:

$$X_G\% = \frac{\sum F_{Ci}}{3*F_{glycerol}}*100$$

where F_{Ci} is the molar flow of the gas products containing carbon – CO, CO_2 and CH_4- and $F_{glycerol}$ is the glycerol molar flow in the feedstock. The selectivity to the gas products denoted as S_{CO}, S_{CO2} and S_{CH4} was calculated as:

$$S_{Ci} = \frac{F_{Ci}}{\sum F_{Ci}}*100$$

The selectivity to H_2 was calculated as:

$$S_{H2} = \frac{F_{H2}}{\sum F_{Ci}}*\frac{3}{7}*100$$

where F_{H2} is the hydrogen molar flow.

The H_2 yield was calculated as:

$$Yield_{H2} = \frac{F_{H2}}{F_{glycerol}}$$

Results and discussion

Support characterization

The composition of the SiO_2-C and C supports was determined by loss on ignition at 800 °C (by TPO/TGA). The weight loss registered for SiO_2-C was 32 wt%, which would correspond to a C/Si ~ 1 mass ratio (Table 1). The C support was prepared by elimination of the silica network by HF acid attack. The weight loss registered for the C support was 85 wt%, which would correspond to a C/Si ~12 mass ratio, thus showing that the HF treatment does not eliminate the Si completely.

The pore size distribution was determined in the 36 to 30,000 Å range, using the mercury intrusion technique. As shown in Fig. 1, both SiO_2-C and C present a very narrow pore size distribution centered at 250 Å for SiO_2-C and 200 Å for C. The commercial Degussa SiO_2 is a non-porous material.

The BET surface area of the supports SiO_2-C and SiO_2 are 255 m^2 g^{-1} and 180 m^2 g^{-1}, respectively (Table 1). To the C support is 1140 m^2 g^{-1}, which represents a value similar to that of commercial carbons. However, commercial carbons generally present an ample pore radius distribution, while support C presents a narrow mesoporous distribution (centered at 200 Å).

The point of zero charge (PZC) is also presented in Table 1. It shows that SiO_2-C and C present a value close to 7, which

Table 1 – Characterization results of the supports.

	SiO_2-C	C	SiO_2
TPO/TGA			
Mass ratio C/Si	1	12	0
Hg intrusion porosimetry			
Max pore rad (Å)	250	200	n.d.
N_2 adsorption–desorption			
S_{BET} (m^2 g^{-1})	255	1140	180
Pore vol (cm^3 g^{-1})	0.40	2.0	0.76
PZC (Point of zero charge)	7	7	2
TPD			
mmolCO_2/g	0.15	0.2	n.d.
mmolCO/g	0.6	3	n.d.

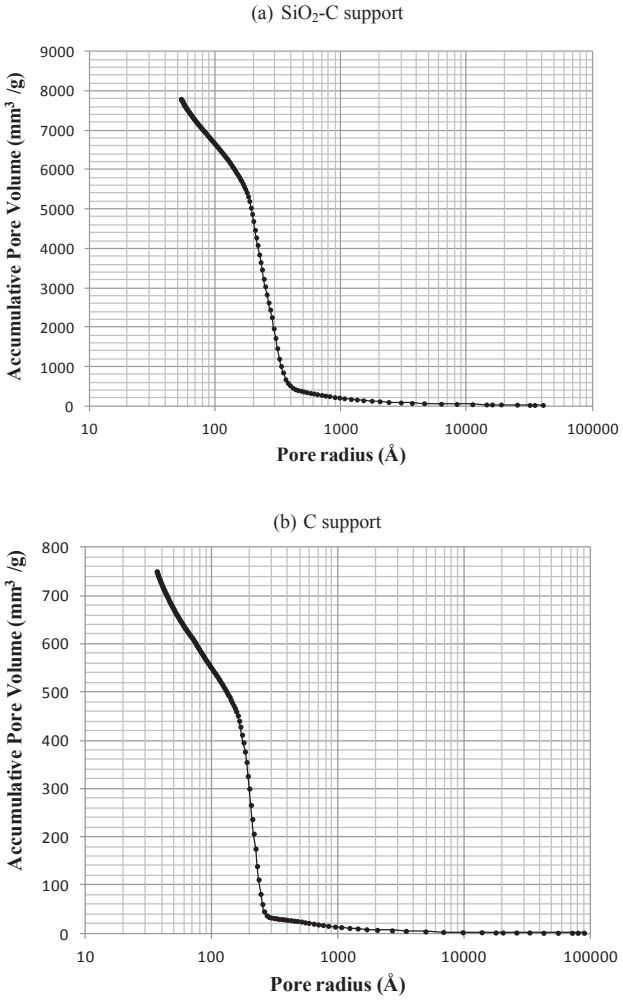

Fig. 1 – Results of mercury intrusion porosimetry. Pore size distribution as cumulative pore volume vs. pore radius of: (a) SiO_2-C and (b) C.

would allow the cationic or anionic exchange with any metallic precursor. On the contrary, SiO_2 presents a PZC value ~2, indicating that SiO_2 acts as a cationic exchanger.

TPD results (Table 1) indicate the amounts of CO and CO_2 released obtained by integrating the areas under TPD peaks. These amounts of CO and CO_2 are very low compared to what was reported by Fraga et al. [39], and would be indicating that supports SiO_2-C and C present low concentrations of surface oxygenated groups. This result seems reasonable if it is taken into account that SiO_2-C and C were subjected to a severe thermal treatment (1500 °C for 3 h) which could have removed most of these surface oxygenated groups.

Fig. 2 shows that the X-ray diffractograms are quite similar in SiO_2-C and C. The presence of a band between $2\theta = 15$ and 30° is observed, characteristic of the silica amorphous band [40,41]. A signal at $2\theta = 43.7°$ assigned to the (1 0 0) plane of the hexagonal phase of graphitic carbon (○) [34,41] can be observed as well as the peaks at $2\theta = 21.8°$, 26.4°, 35.7°, 41.4°, 60.0° and 71.9° assigned to the (0 0 4 8), (0 1 1), (1 1 1), (2 0 0), (2 2 0) and (3 1 1) planes of silicon carbide (Δ) (JCPDS 29-118, JCPDS 29-129) [42,43]. The peaks corresponding to the graphitic carbon hexagonal phase (1 0 2), (0 0 4) and (1 0 3) at $2\theta = 51°$, 54.5°, 59° respectively cannot be distinguished. This could be due to the formation of turbostratic carbon. In the literature, it has been reported that turbostractic carbon is a graphitic carbon whose structural planes are rotated and translated with respect to their normal conformation. The presence of turbostractic carbon provokes a shift of the peaks to lower angular values of 2θ and, in this case, they could overlap the silica amorphous band [44].

In previous work, we have shown that the supports with neutral properties such as SiO_2 reduce the formation of side products coming from the dehydration and condensation reactions leading to coke deposition [28]. In order to characterize the surface acidity properties of the supports, we employed an indirect method by the catalytic decomposition reaction of isopropanol (IPA). As demonstrated by Gervasini et al. [38], the isopropanol dehydration (that produces propylene and/or di-isopropylether is catalyzed by acid sites). The dehydrogenation (that produces ketone), in the absence of metals, is catalyzed by acid and basic sites through a concerted mechanism and serves as basicity measure of the materials analyzed. Table 2 shows the isopropanol conversion (X_{IPA})

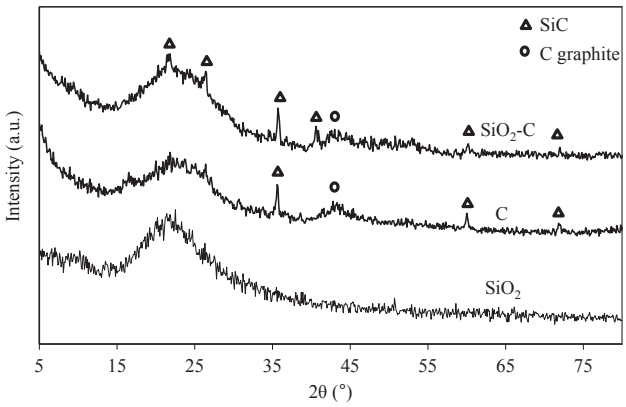

Fig. 2 – XRD patterns of SiO_2-C, C and SiO_2 supports.

Table 2 – Results of isopropanol (IPA) decomposition reaction. Data collected at 260 °C. atmospheric pressure, feed 4.5% IPA in Helium with a flow 40 cm^3 min^{-1}.

	Conversion (%)	Selectivity (%)		
	X_{IPA}	$S_{propylene}$	$S_{acetone}$	$S_{di\text{-}isopropylether}$
SiO_2	5	7	93	0
C	24	96	3	1
SiO_2-C	6	51	47	2

results at 260 °C. For SiO_2-C and SiO_2 supports, conversions are low ($X_{IPA} \leq 6\%$), evidencing a low concentration of superficial active sites. For the SiO_2-C support, the selectivity towards propylene and acetone is similar which indicates the presence of weak Lewis acid sites. The C support presents the highest activity, which demonstrates the greater number of surface active sites, and the higher selectivity towards propylene would indicate a greater contribution of strong Lewis acid sites or Brønsted acid sites.

The presence of di-isopropylether in very low amounts indicates a low concentration of strong Lewis acid sites.

Catalyst characterization

Table 3 shows the characterization results of catalysts Pt/SiO_2-C, Pt/C and Pt/SiO_2. The metallic content determined by AAS is very close to 2 wt%. The high dispersion of the particles in Pt/SiO_2-C was determined by TEM (Fig. 3), with the presence of small metallic particles of around 1.4 nm ($d_{va} = 1.37$ nm). The dispersion of Pt/C is slightly lower, with an average particle size of around 1.5 nm ($d_{va} = 1.49$ nm). The Pt/SiO_2 catalyst presents the lowest metallic dispersion, with an average particle size of 2.2 nm ($d_{va} = 2.16$ nm).

For metallic catalysts supported on carbonaceous materials, it is important to determine the thermal stability of the support. Typical TPO curves for carbonaceous materials heated under an oxidative atmosphere are presented in Fig. 4. During the carbon regeneration process, Matatov-Meytal et al. characterized two typical temperatures: the carbon "activation" temperature (Tc) and the "burn-off" temperature (Tg) [45]. The lowest temperature (Tc) corresponds to the temperature at which oxygen attacks the carbon surface and surface oxidation begins (also known as carbon activation). The highest temperature (Tg) corresponds to the oxidation of the C skeleton, also called burn-off or carbon gasification.

Fig. 4 shows the TPO/MS results for catalysts Pt/C and Pt/SiO_2-C. For the Pt sample, Tc = 460 °C and Tg = 500 °C can be observed, while for sample Pt/SiO_2-C, Tc = 520 °C and Tg = 640 °C are shown. This indicates that the presence of Si in the SiO_2-C sample delays the gasification of C in approximately 140 °C.

Table 3 – Results of Pt content by AAS and characterization by TEM of Pt catalysts.

	Pt/SiO_2-C	Pt/C	Pt/SiO_2
%wt Pt (AAS)	1.9	1.8	2
d_{va} (nm)*	1.37	1.49	2.16
D_{TEM} (%)**	78.8	72.5	50

Where, * $d_{va} = \frac{\sum ni \cdot di^3}{\sum ni \cdot di^2}$ and ** $D_{TEM} = \frac{108}{d_{va}} \times 100$

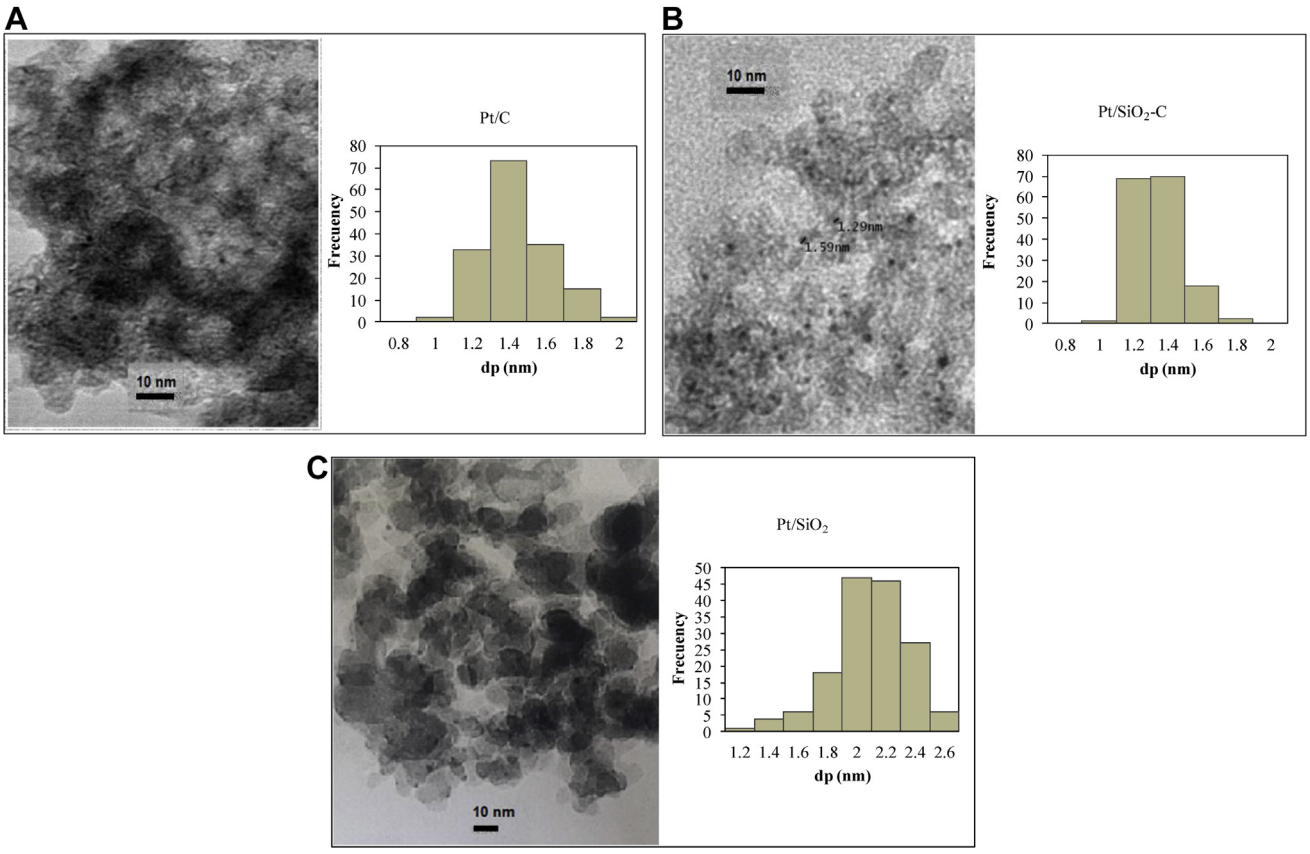

Fig. 3 – Particle size distribution determined by transmission electron microscopy (TEM) of: a) Pt/C, b) Pt/SiO_2-C, c) Pt/SiO_2.

TPR results are shown in Fig. 5. The results of Pt/SiO_2 show a low temperature peak at 180 °C and a second reduction event at 405 °C. For Pt/SiO_2 catalysts, Ho et al. reported that the species with more interaction Pt-(O-Si ≡)$_y^{n-y}$ (n = +2 or +4) are reduced to temperatures in the 400–500 °C range [46].

The TPR profile of Pt/C also shows the consumption of hydrogen at two temperature regions. In the region at 150 °C, there is only H_2 consumption and the peak is attributed to Pt reduction. According to the literature, the lowest temperature peak can be assigned to the reduction of Pt oxide species weakly interacting with the support [46,47]. The signal at a higher temperature, 640 °C, corresponds to the consumption of H_2 and the release of CO. For this reason, this peak is assigned to H_2 consumption by unsaturated sites and to the decomposition of the surface oxygenated groups of the C support.

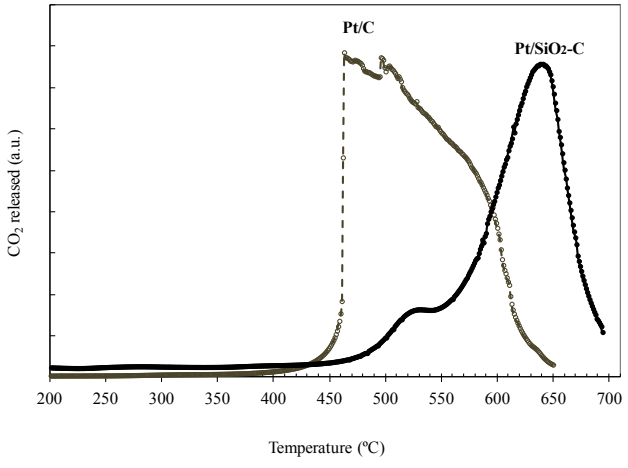

Fig. 4 – Temperature-programmed oxidation (TPO/MS). TPO profiles (in 5 v/v% O_2 and Ar flow) of Pt/C and Pt/SiO_2-C.

In the Pt/SiO_2-C sample, two Pt reduction events can be distinguished, the low temperature signal at 200 °C and the signal in the 460–520 °C range assigned to Pt species with a higher interaction than in Pt/SiO_2.

In order to determine the H_2 consumption corresponding to platinum reduction, the region between 200 and 560 °C was considered. For the quantification, a calibration curve with CuO was employed and the platinum reduction was close to 94–97% for all catalysts.

The XPS results are summarized in Table 4 and Fig. 6 where the binding energy (BE) of the Pt4f$_{5/2}$ and Pt4f$_{7/2}$ are shown. In all the samples, the presence of Pt(0) and Pt(II) were detected, even in the PtSiO_2-C sample treated in Ar at 350 °C. This would be implying that the Pt(IV) reduction occurs during the preparation stage. It has been reported in the literature that Pt(IV) is reduced even during the impregnation step due to the presence of surface oxygen groups of carbonaceous supports [48].

The PtSiO_2 sample was reduced in situ at 350 °C and the spectra only show the presence of Pt(0). The results of the PtSiO_2-C and Pt-C samples, pre-reduced ex-situ at 350 °C, show the presence of Pt (II) which could be due to oxidation by exposure to the atmosphere. The intensity of the surface Pt

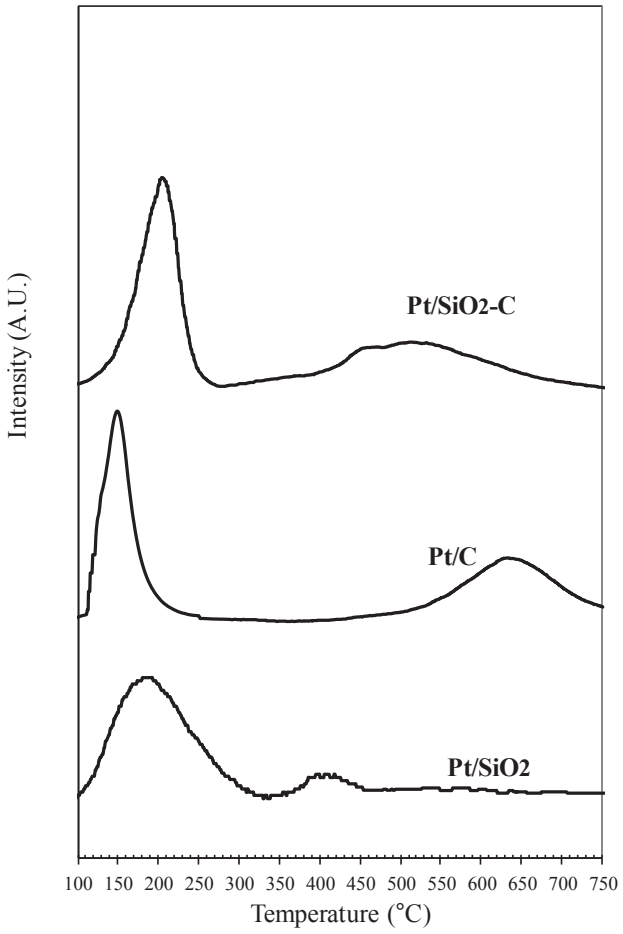

Fig. 5 – Temperature-programmed reduction (TPR) profiles of Pt/SiO_2-C, Pt/C, and Pt/SiO_2 catalysts.

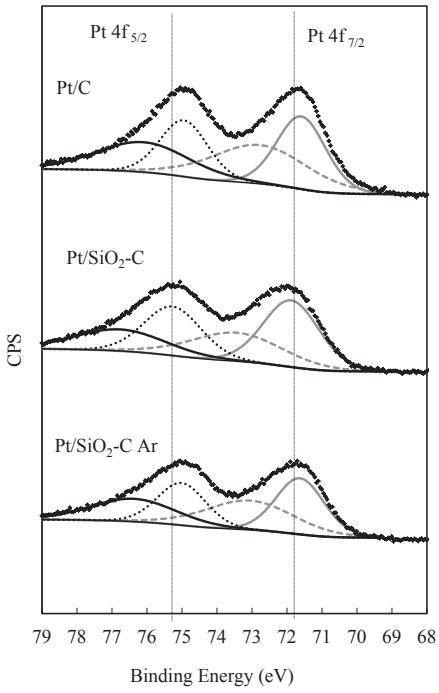

Fig. 6 – XPS spectra of Pt$4f_{5/2}$ and $4f_{7/2}$ level for PtSiO_2-C and Pt/C catalysts.

signal for Pt/SiO_2 is the lowest one (Table 4), which is in agreement with the results of metallic dispersion.

Catalytic performance

According to various authors, in order to obtain the best yields towards hydrogen the working temperature range should be between 550 and 750 °C [6,7,49]. However, reducing the reaction temperature not only reduces energy consumption but also prevents catalyst sintering.

Taking into account that glycerol is not a thermally stable molecule and that it can decompose, a preliminary test without catalyst has been carried out to ascertain the extent of pyrolysis phenomena. The blank test performed at 450 °C using a reaction stream containing 30 wt% of glycerol, indicated that the thermal decomposition of glycerol was lower than 5% molar. The main decomposition products were acetol, 2-oxopropanal and acetaldehyde. If the temperature increased, the thermal decomposition of glycerol could reach 30% molar at a temperature of 650 °C.

The selection of the operating conditions to evaluate the catalytic performance in the glycerol steam reforming reaction is available in the supplementary information.

The activity results in the glycerol steam reforming at 450 °C, steam/carbon molar ratio (S/C) ~ 4 and WHSV (weight hourly space velocity, calculated as the mass flow rate of glycerol into the reactor divided by the mass of catalyst) = 14.7 h^{-1} (Table 5) show that catalysts Pt/SiO_2-C and Pt/C reach glycerol gas conversions of 83 and 85%, respectively, while the Pt/SiO_2 catalyst presents a conversion of 64%. Thus, the catalysts with the highest metallic dispersion, Pt/SiO_2-C and Pt/C, present the greatest selectivity to H_2.

Table 6 shows the activity results of the Pt/SiO_2-C catalyst at different WHSV and steam/carbon ratio (S/C) in the feeding. It can be observed that, by keeping WHSV practically constant (between 5 and 5.7 h^{-1}), as the S/C ratio decreases, SCO increases and SCO_2 decreases due to the fact that the WGS reaction is disfavored. Besides, it can also be seen that with the decrease of WHSV, from 5.7 to 2.9 h^{-1}, for S/C = 4 i.e.,

Table 4 – XPS of Pt $4f_{7/2}$ and $4f_{5/2}$ region of Pt catalysts.

Sample	Pt/C	Pt/Si	C/Si	Pt (II)/Pt (0)	Pt (0)/Pt total
Pt/SiO_2-C (Ar)	0.006	0.032	5.320	0.960	0.51
Pt/SiO_2-C	0.008	0.042	5.236	0.786	0.56
Pt/SiO_2	–	0.024	–	–	1
Pt/C	0.008	–	–	1.040	0.49

Table 5 – Results of GSR reaction at 450 °C, WHSV = 14.7 h^{-1} and 2 h on stream.

Catalyst	$X_{glycerol}$	SH_2	SCO	SCO_2	SCH_4	Yield H_2
Pt/SiO_2-C	83	51	78.0	16.6	5.4	3.0
Pt/C	85	52	87.5	8.7	3.8	3.1
Pt/SiO_2	64	38.8	73.3	24.2	2.5	1.7

Table 6 – Results of GSR reaction of the Pt/SiO_2-C catalyst, at 450 °C and 2 h on stream.

Ratio steam/carbon	WHSV (h^{-1})	$X_{glycerol}$	SH_2	SCO	SCO_2	SCH_4	Yield H_2	H_2/CO	CO/CO_2
		(%)							
S/C = 15	5	98	60	46	48	6	4.1	3.4	1
S/C = 4	25.7	70	43	81	13.8	5.2	2.1	1.9	4
	14.7	83	51	78	16.6	5.4	3	1.85	4.7
	5.7	100	68.8	52.5	41.7	5.8	4.8	3.1	1.3
	2.9	100	74.7	32.4	61.8	5.8	5.2	5.4	0.5
S/C = 1.6	5	96	63	58	33	9	4.2	2.7	1.8

conversion remains similar but the H_2 yield and SCO_2 increase due to the competition between glycerol and CO for the same active sites.

Due to the different experimental conditions employed by other authors, it is difficult to compare our results with other Pt catalysts reported in the literature. Kunkes et al. reported catalysts of Pt/C and Pt-Re/C with 5 wt% of Pt, evaluated in GSR at 275 °C, atmospheric pressure, 30 wt% glycerol (S/C = 4) and WHSV = 1.6 h^{-1} [48]. The higher metallic charge, the smallest WHSV employed and the presence of Re in the Pt catalyst, allowed these authors to obtain a reaction product with a high H_2/CO = 4.3 ratio and a low CO/CO_2 = 0.65 ratio, which can be explained by a greater contribution of the WGS reaction. Doukkali et al. [50] studied Pt and PtNi catalysts supported on γ-Al_2O_3 modified by La and Ce oxides, with 2.5 wt% Pt and 12.5 wt% Ni. At 450 °C, WHSV = 5.85 h^{-1} and a S/C = 18 ratio, the PtNi bimetallic catalysts were the most active ones, with 100% conversion to gases and hydrogen yields between 4.2 and 4.4.

If the behavior of catalysts Pt/SiO_2-C, Pt/C and Pt/SiO_2 with time on stream is analyzed, these materials present considerable differences (Fig. 7). It is possible to observe that catalysts Pt/SiO_2 and Pt/C lose approximately half their initial activity in a period of 16 h and 35 h, respectively.

Catalyst Pt/SiO_2 deactivates after the first 8 h on stream when a S/C = 4 ratio is employed (Fig. 7). The TEM characterization of the Pt/SiO_2 spent sample (Table 7) indicates an

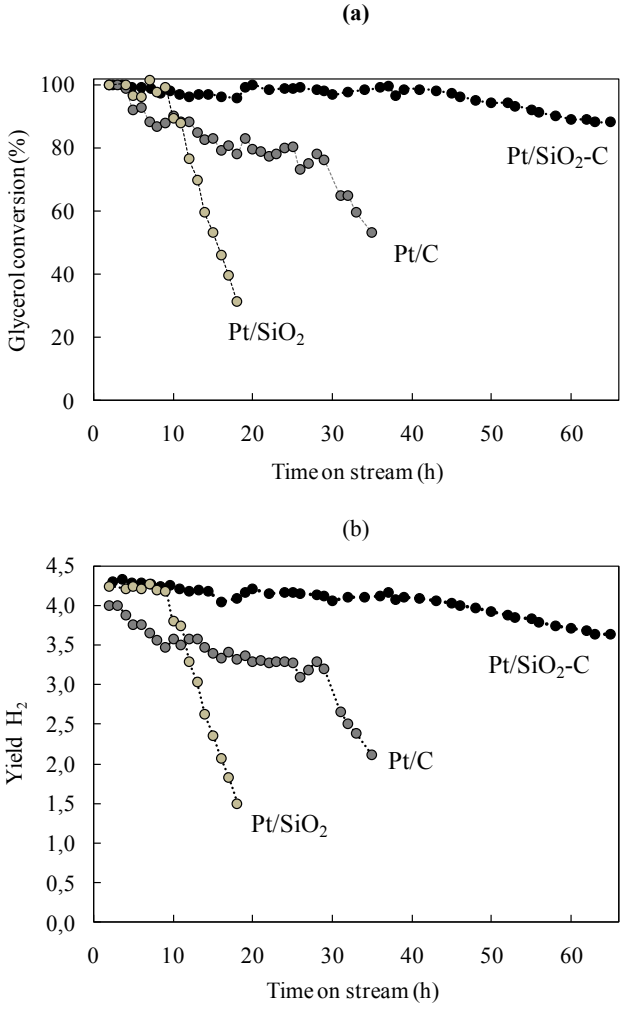

Fig. 7 – Glycerol conversion (a) and Yield H_2 (b) as a function of reaction time; at 450 °C, WHSV = 8.7 h^{-1}, and S/C = 4.

Table 7 – Characterization results of spent samples.

	Spent sample		
	Pt/SiO_2	Pt/C	Pt/SiO_2-C
TEM			
dav (nm)	2.4	2.8	1.5
TPO/TGA			
%C	2	n.d.	n.d.
XPS			
atomic surface ratio Pt/C	n.d.	n.d.	0.005
atomic surface ratio Pt/Si			0.030

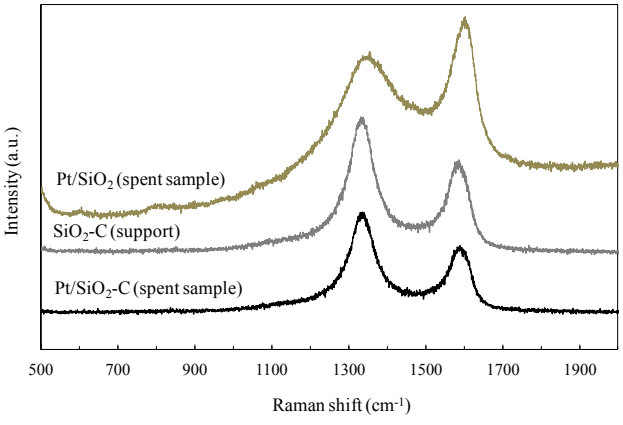

Fig. 8 – Laser Raman spectra of $PtSiO_2$ and $PtSiO_2$-C samples.

average particle size of $d_{va} = 2.4$ nm, very similar to that of the fresh catalyst (2.2 nm) and allows discarding sintering as the main deactivation cause.

By TPO/TGA it was determined that the Pt/SiO_2 spent sample had 2 wt% of C and that the burning temperature was approximately 500 °C. The rate of carbon formation, calculated considering the amount of carbon deposited along 18 h of reaction, was 1 mg C g_{cat}^{-1} h^{-1}, which is considerably slower than the 4 mg C $g_{cat}^{-1}h^{-1}$rate reported by Chiodo et al. for the Ni/CeO_2 catalyst [32]. Besides, the low burning temperatures of the carbon deposited (~500 °C) would suggest that the carbon is of the encapsulating type, typical of high reactivity carbon, which is highly deactivating. This would explain the rapid deactivation of the Pt/SiO_2 catalyst. This has already been discussed by Doukkali et al., who reported a Pt catalyst supported on alumina that presented a strong deactivation provoked by the low content of encapsulating carbon [50].

With respect to the Pt/C catalyst, the TEM characterization of the spent sample shows that it has an average particle size of $d_{va} = 2.8$ nm. This would correspond to a 50% loss of the metallic dispersion in 35 h on stream and could suggest that sintering contributes strongly to the deactivation of this catalyst. However, due to the more acid features of the C support compared to those of SiO_2 and SiO_2-C, the formation of coke on this catalyst is not ruled out.

As shown in Fig. 4, the initial combustion temperature of the carbon support is 460 °C for Pt/C and 520 °C for Pt/SiO_2-C. Therefore, it is not possible to determine the coke content by TPO/TGA in these used catalysts since the support combustion occurs at the same temperature as the coke burning.

Fig. 7 shows that the most stable catalyst was Pt/SiO_2-C, which lost only 10% of its initial activity after 66 h on stream. The TEM characterization of the Pt/SiO_2-C spent sample reveals that it has an average particle size of $d_{va} = 1.5$ nm, quite similar to that of the fresh catalyst (1.37 nm), indicating its high resistance to sintering due to the greater interaction of Pt with the SiO_2-C support.

The carbon deposits of the used samples were characterized by Raman analysis (Fig. 8). The D and D′ bands, at 1360 and 1610 cm^{-1} respectively, are assigned to amorphous carbon and the G band (related to the stretching vibration mode E2g in C=C (C sp^2) bond) at 1580 cm^{-1} corresponds to graphitic carbon [51].

Fig. 8 shows that in the Pt/SiO_2 spent sample, the Raman signals appearing at 1360 and 1610 cm^{-1} are typical of the non-crystalline carbon deposits. The Raman spectra of the Pt/SiO_2-C spent sample and of the SiO_2-C support are quite similar and for this reason, it is not possible to distinguish between the carbon deposited and the carbon from the support.

The XPS analysis of the Pt/SiO_2-C spent sample (Table 7) reveals a slight decrease of the Pt surface signal, which would be in agreement with a slight sintering and a slight coverage of the Pt particles by carbon deposits. In this way, the presence of small metallic particles in Pt/SiO_2-C not only favors the C–C bond cleavage reactions to produce hydrogen but also prevents the formation of coke precursors and their deposition.

Conclusions

The Pt/SiO_2-C catalyst results of interest for glycerol steam reforming at low temperature due to the characteristics of the support and of the metallic particles obtained. On the one hand, the SiO_2-C support presents a high specific surface area due to its mesoporosity and its lack of surface acidity, which avoids the dehydration reactions that are damaging for coke formation. On the other hand, the metallic particles are very well dispersed which favors the cleavage reactions of the C–C bonds and have a good interaction with the support, which makes them highly resistant to sintering. These characteristics allow the Pt/SiO_2-C catalyst to reach not only high levels of selectivity to H_2 but also a slower rate of carbon deposition.

Acknowledgments

We thank financial support received from CONICET (PIP 611) and UNLP (I-175).

Appendix A. Supplementary data

Supplementary data related to this article can be found at http://dx.doi.org/10.1016/j.ijhydene.2017.04.047.

REFERENCES

[1] Argentina; Federal Law Number 26093. Regulation and promotion for the sustainable production and use of biofuels. 2006. Available at: http://servicios.infoleg.gob.ar/infolegInternet/anexos/115000-19999/116299/norma.htm.
[2] Argentina; Ministry of Energy and Mining. Biofuels statistics. 2017. Available at: http://www.energia.gob.ar.
[3] Serrano-Ruiz JC, Luque R, Sepúlveda-Escribano A. Transformations of biomass-derived platform molecules: from high added-value chemicals to fuels via aqueous-phase processing. Chem Soc Rev 2011;40:5266–81.
[4] Pastor-Pérez L, Sepúlveda-Escribano A. Low temperature glycerol steam reforming on bimetallic PtSn/C catalysts: on the effect of the Sn content. Fuel 2017;194:222–8.
[5] Li D, Li X, Gong J. Catalytic reforming of oxygenates: state of the art and future prospects. Chem Rev 2016;116:11529–653.
[6] Schwengber CA, Alves HJ, Schaffner RA, Alves da Silva F, Sequinel R, Rossato V, et al. Overview of glycerol reforming for hydrogen production. Renew Sust Energy Rev 2016;58:259–66.
[7] Dou B, Song Y, Wang C, Chen H, Xu Y. Hydrogen production from catalytic steam reforming of biodiesel byproduct glycerol: issues and challenges. Renew Sust Energy Rev 2014;30:950–60.
[8] Luo N, Zhao X, Cao F, Xiao T, Fang D. Thermodynamic study on hydrogen generation from different glycerol reforming processes. Energy Fuels 2007;21:3505–12.
[9] Adhikari S, Fernando S, Gwaltney SR, Filip To SD, Mark Bricka R, Steele PH. A thermodynamic analysis of hydrogen production by steam reforming of glycerol. Int J Hydrogen Energy 2007;32:2875–80.

[10] Soares RR, Simonetti DA, Dumesic JA. Glycerol as a source for fuels and chemicals by low-temperature catalytic processing. Angew Chem Int Ed 2006;45:3982–5.
[11] Simonetti DA, Kunkes EL, Dumesic JA. Gas-phase conversion of glycerol to synthesis gas over carbon supported platinum and platinum rhenium catalysts. J Catal 2007;247:298–306.
[12] Montini T, Singh R, Das P, Lorenzut B, Bertero N, Riello P. Renewable H_2 from glycerol steam reforming: effect of La_2O_3 and CeO_2 addition to Pt/Al_2O_3 catalysts. Chem Sus Chem 2010;3:619–28.
[13] Sutar PN, Vaidya PD, Rodrigues AE. Glycerol-reforming kinetics using a Pt/C catalyst. Chem Eng Technol 2010;33:1645–9.
[14] Iulianelli A, Seelam PK, Liguori S, Longo T, Keiski R, Calabro V. Hydrogen production for PEM fuel cell by gas phase reforming of glycerol as by product of bio-diesel. Int J Hydrogen Energy 2011;36:3827–34.
[15] Cheng CK, Foo SY, Adesina AA. Steam reforming of glycerol over Ni/Al_2O_3 catalyst. Catal Today 2011;178:25–33.
[16] Cheng CK, Foo SY, Adesina AA. Glycerol steam reforming over bimetallic $CoNi/Al_2O_3$. Ind Eng Chem Res 2010;49:10804–17.
[17] de Rezende SM, Franchini CA, Dieuzeide ML, Duarte de Farias AM, Amadeo N, Fraga MA. Glycerol steam reforming over layered double hydroxide-supported Pt catalysts. Chem Eng J 2015;272:108–18.
[18] Wei Z, Karim AM, Li Y, King DL, Wang Y. Elucidation of the roles of Re in steam reforming of glycerol over Pt–Re/C catalysts. J Catal 2015;322:49–59.
[19] Soares RR, Martins DF, Pereira DES, Almeida MB, Lam YL. On the gas-phase reforming of glycerol by Pt on carbon black: effects of metal particle size and pH value of the glycerol stream. J Mol Catal A Chem 2016;422:142–7.
[20] Lin KH, Chang ACC, Lin WH, Chen S, Chang CY, Chang HF. Autothermal steam reforming of glycerol for hydrogen production over packed-bed and Pd/Ag alloy membrane reactors. Int J Hydrogen Energy 2013;38:12946–52.
[21] Huang X, Dang C, Yu H, Wang H, Peng F. Morphology effect of $Ir/La_2O_2CO_3$ nanorods with selectively exposed {110} facets in catalytic steam reforming of glycerol. ACS Catal 2015;5:1155–63.
[22] Araque M, Martínez LM, Vargas JC, Centeno MA, Roger AC. Effect of the active metals on the selective H2 production in glycerol steam reforming. App Catal B Environ 2012;125:556–66.
[23] González-Gil R, Chamorro-Burgos I, Herrera C, Larrubia MA, Laborde M, Mariño F, et al. Production of hydrogen by catalytic steam reforming of oxygenated model compounds on Ni-modified supported catalysts. Simulation and experimental study. Int J Hydrogen Energy 2015;40:11217–27.
[24] Martínez LM, Araque M, Centeno MA, Roger AC. Role of ruthenium on the catalytic properties of CeZr and CeZrCo mixed oxides for glycerol steam reforming reaction toward H2 production. Catal Today 2015;242:80–90.
[25] Gallo A, Pirovano C, Ferrini P, Marelli M, Psaro R, Santangelo S, et al. Influence of reaction parameters on the activity of ruthenium based catalysts for glycerol steam reforming. Appl Catal B 2012;121:40–9.
[26] Buffoni IN, Pompeo F, Santori GF, Nichio NN. Nickel catalysts applied in steam reforming of glycerol for hydrogen production. Catal Commun 2009;10:1656–60.
[27] Cheng CK, Foo SY, Adesina AA. H2-Rich synthesis gas production over Co/Al2O3 catalyst via glycerol steam reforming. Catal Commun 2010;12:292–8.
[28] Pompeo F, Santori G, Nichio N. Hydrogen and/or syngas from steam reforming of glycerol. Study of platinum catalysts. Int J Hydrogen Energy 2010;35:8912–20.
[29] Wu G, Li S, Zhang C, Wang T, Gong J. Glycerol steam reforming over perovskite-derived nickel-based catalysts. Appl Catal B Environ 2014;144:277–85.
[30] Wu G, Zhang C, Li S, Han Z, Wang T, Ma X, et al. Hydrogen production via glycerol steam reforming over Ni/Al2O3: influence of nickel precursors. ACS Sustain Chem Eng 2013;1:1052–62.
[31] Li S, Gong J. Strategies for improving the performance and stability of Ni-based catalysts for reforming reactions. Chem Soc Rev 2014;43:7245–56.
[32] Chiodo V, Freni S, Galvagno A, Mondello N, Frusteri F. Catalytic features of Rh and Ni supported catalysts in the steam reforming of glycerol to produce hydrogen. Appl Catal A Gen 2010;381:1–7.
[33] Araque M, Martinez LM, Vargas JC, Roger AC. Hydrogen production by glycerol steam reforming over CeZrCo fluorite type oxides. Catal Today 2011;176:352–6.
[34] Lombardi B, Pompeo F, Scian AN, Nichio NN. High specific surface area of SiO_2–C meso-and nanoporous materials textural assessment and surface development. Matt Lett 2013;106:393–5.
[35] Li N, Hu Z, Zheng M, Lu H, Zhao B, Zhang S, et al. Formation of Pt nanoparticles in mesoporous silica channels via direct low-temperature decomposition of $H_2PtCl_6 \cdot 6H_2O$. Matt Lett 2013;106:193–6.
[36] Goguet A, Aouine M, Cadete Santos Aires FJ, De Mallmann A, Schweich D, Candy JP. Preparation of a Pt/SiO_2 catalyst: I. Interaction between platinum tetrammine hydroxide and the silica surface. J Catal 2002;209:135–44.
[37] Richard MA, Pancirov R. Thermal decomposition of tetraamineplatinum (II) chloride by simultaneous TG/DTG/DTA/MS and direct insertion probe mass spectrometry. J Therm Anal 1987;32:825–34.
[38] Gervasini A, Fenyvesi J, Auroux AA. Study of the acidic character of modified metal oxide surfaces using the test of isopropanol decomposition. Catal Lett 1997;43:219–28.
[39] Fraga M, Jordão E, Mendes M, Freitas M, Faria J, Figueiredo J. Properties of carbon-supported platinum catalysts: role of carbon surface sites. J Catal 2002;209:355–64.
[40] Ding H, Li J, Gao Y, Zhao D, Shi D, Mao G, et al. Preparation of silica nanoparticles from waste silicon sludge. Powder Technol 2015;284:231–6.
[41] Niu T, Liu GL, Liu Y. Preparation of Ru/graphene-meso-macroporous SiO_2 composite and their application to the preferential oxidation of CO in H_2-rich gases. Appl Catal B Environ 2014;154:82–92.
[42] Dong R, Yang W, Wu P, Hussain M, Xiu Z, Wu G, et al. Microstructure characterization of SiC nanowires as reinforcements in composites. Mat Charact 2015;103:37–41.
[43] Omidin Z, Ghasemi A, Bakhshi S. Synthesis and characterization of SiC ultrafine particles by means of sol-gel and carbothermal reduction methods. Ceram Int 2015;41:5779–84.
[44] Li ZQ, Lu CJ, Xia ZP, Zhou Y, Luo Z. X-ray diffraction patterns of graphite and turbostratic carbón. Carbon 2007;45:1686–95.
[45] Matatov-Meytal Y, Sheintuch M, Shter GE, Grader GS. Optimal temperatures for catalytic regeneration of activated carbon. Carbon 1997;35:1527–31.
[46] Ho LW, Hwang CP, Lee JF, Wang I, Yeh CT. Reduction of platinum dispersed on dealuminated beta zeolite. J Mol Catal A Chem 1998;136:293–9.
[47] Jongpatiwut S, Rattanapuchapong N, Rirksomboon T, Osuwan S, Resasco S. Enhanced sulfur tolerance of bimetallic $PtPd/Al_2O_3$ catalysts for hydrogenation of tetralin by addition of fluorine. Catal Lett 2008;122:214–22.
[48] Kunkes EL, Simonetti DA, Dumesic JA, Pyrz WD, Murillo LE, Chen JG, et al. The role of rhenium in the conversion of

glycerol to synthesis gas over carbon supported platinum–rhenium catalysts. J Catal 2008;260:164–77.
[49] Lin YC. Catalytic valorization of glycerol to hydrogen and syngas. Int J Hydrogen Energy 2013;38:2678–700.
[50] El Doukkali M, Iriondo A, Arias PL, Cambra JF, Gandarias I, Barrio VL. Bioethanol/glycerol mixture steam reforming over Pt and PtNi supported on lanthana or ceria doped alumina catalysts. Int J Hydrogen Energy 2012;37:8298–309.
[51] Arepalli S, Nikolaev P, Gorelik O, Hadjiev V, Holmes W, Files B, et al. Protocol for the characterization of single-wall carbon nanotube material quality. Carbon 2004;42:1783–91.